

**25-Day Period Large-Scale Oscillations in the Argentine Basin Revealed by the
TOPEX/POSEIDON Altimeter**

Lee-Lueng Fu and Benny Cheng

Jet Propulsion Laboratory
California Institute of Technology
4800 Oak Grove Drive, MS 300-323
Pasadena, CA 91109

Bo Qiu

Department of Oceanography
University of Hawaii
1000 Pope Road
Honolulu, HI 96822

July, 1999

Abstract

The measurement of global sea surface height made by the TOPEX/POSEIDON satellite has provided the first synoptic view of large-scale oceanic variability at the intraseasonal scales from weeks to months. Areas of significant intraseasonal variability were primarily found in the high-latitude oceans, the Southern Ocean in particular. The focus of the paper is the finding of large-scale oscillations at a period of 25 days in the Argentine Basin of the South Atlantic Ocean. These oscillations exhibit a pattern of counter-clockwise rotational propagation centered at 45° S and 317° E over the Zapiola Rise, with a half wavelength of about 1000 km. The peak-to-trough amplitude is about 10 cm. The amplitude of these waves has large seasonal-to-interannual variations. These oscillations are shown to be a free barotropic mode of the basin as a solution to a linearized barotropic vorticity equation. Closed f/H contours provide a mechanism for the confinement of the waves to the topographic feature of the Zapiola Rise. Results from a numerical model simulation reproduced the observed pattern of the waves. The barotropic nature of the variability yields an estimate of the amplitude of the mass transport variation to be about 50 Sv. Deep current meters in the Argentine Basin reveal signals that are consistent with the altimetry observations.

1. Introduction

The intraseasonal variability of sea level, characterized by time scales between a few days and the seasonal scale, and by spatial scales larger than 500 km, the upper bound of the mesoscale, has not been observed adequately until the advent of precision altimetric missions such as TOPEX/POSEIDON. In-situ observations in the tropics are an exception for several reasons, however. First, most mid-ocean island tide gauges are located in the tropics. Second, intraseasonal variabilities in the tropics are particularly energetic. Third, the mesoscale eddies are relatively weak in the tropics and hence are not an impediment to observing the intraseasonal scales. The tropical intraseasonal variability has been interpreted primarily as an ocean's response to the atmospheric forcing in terms of internal gravity waves as well as Kelvin, Rossby, and instability waves (e.g., Wunsch and Gill, 1976; Enfield, 1987; McPhaden, 1996). The scarce in-situ observations at mid and high latitudes have prevented a detailed description of sea level variability at the intraseasonal scales. The ubiquitous mesoscale eddies often make the signal-to-noise ratio fairly low for detecting large-scale intraseasonal variabilities. Using a large number of deep current meter observations, Koblinsky et al. (1989) demonstrated the existence of large-scale response of the ocean to local wind forcing at the intraseasonal scales. Other studies reported evidence of remotely forced large-scale response of the ocean to wind forcing as barotropic Rossby waves (Brink, 1989; Niiler et al., 1993; Samelson, 1990; Luther et al., 1990) However these in-situ observations are not able to provide a coherent, synoptic view of these large-scale variabilities. Because these variabilities occur on relatively short time scales, repeated transocean shipboard measurements are not frequent enough to sample them.

With its unique spatial and temporal sampling capability, satellite altimetry offers an effective approach to the problem. However, the relatively low amplitude (less than 10 cm) and large scales (greater than 500 km) of the variability present a challenge to the performance of altimetric measurement. Before the advent of the T/P mission, the orbit errors in altimetric measurement are much larger than 10 cm. Because the spatial scales of orbit errors are rather large (predominantly on the order of the circumference of Earth), small-scale signals can be preserved after the removal of the orbit errors by fitting the large-scales to an orbit error model (Fu and Vazquez, 1988; Wagner and Tai, 1994). Such procedures often create distortion of the signals at large scales and compromise the data quality for studying the intraseasonal variability. With its orbit accuracy better than 4 cm (Fu et al., 1994), T/P provides the first opportunity for observing the large-scale patterns of the variability.

Shown in Figure 1 is the standard deviation of sea level variability at spatial scales larger than 1000 km and temporal scales between 20 and 100 days determined from the T/P altimeter observations as well as from an ocean general circulation model (from Fu and Smith, 1996). The energy level is generally low with an rms amplitude of 2-3 cm. The maximum amplitude is in the Southern Ocean with rms magnitude greater than 3 cm and peak-to-trough sea level variations exceeding 10 cm in certain regions. The geographic distribution of the energy level is well reproduced by the model (also see Chao and Fu, 1995). In the Northern Hemisphere where the wind forcing is relatively well known, the model is able to simulate the temporal evolution of the variability with a high degree of correlation with observed sea level time series. Chao and Fu (1995) also showed that the

model-simulated sea level was highly correlated with the model's barotropic stream function, suggesting that the variability was caused by barotropic motions. Fu and Davidson (1995) made an attempt to describe the observed variability in terms of a wind-driven linearized barotropic vorticity equation without much success. Fukumori et al. (1998) presented a more detailed account of the barotropic nature of the variability using an ocean general circulation model.

The details of the intraseasonal variability revealed in the T/P data have not been investigated. In this paper we present results from the investigation of a particular mode of variability in the Argentine Basin of the South Atlantic Ocean where the observed intraseasonal variability has the highest energy level according to Figure 1. The variability of the circulation of the Argentine Basin has been documented by many previous studies. The region exhibits a high degree of variability over a wide range of space and time scales. The eddy energy level in the Brazil/Malvinas Confluence region is among the highest in the world's oceans (Provost and Le Traon, 1993), with an rms sea level variability greater than 30 cm. Large-scale annual and semi-annual cycles are also prominent with a sea level amplitude of 13 and 7 cm, respectively (Fu, 1996; Provost and Le Traon, 1993). There have been numerous observational and theoretical studies of the eddy and seasonal variabilities of the region (Olson et al., 1988; Garzoli and Garaffo, 1989; Matano et al., 1993; Garzoli and Giulivi, 1994). Recently, the large-scale interannual variability of the South Atlantic was investigated by Witter and Gordon (1999) using T/P data. They discovered a distinct interannual mode in the Brazil/Malvinas Confluence region.

There has been little discussion of the intraseasonal variability in the Argentine Basin in the literature. Weatherly (1993) reported the findings of high-frequency (periods of 22-28 days) oscillations in the observations made by current meters near the ocean bottom close to the Zapiola Rise, a sediment ridge located along 45° S from 315°-320°. He suspected that these oscillations were due to large-scale barotropic Rossby waves. In this paper we present a detailed view of the spatial and temporal characteristics of such waves from multiple years of T/P data.

2. Data Processing

T/P measures the sea surface height (SSH) every 6.2 km along repeat ground tracks every 10 days. The longitudinal distance between ground tracks is approximately 200 km at the latitude of the Argentine Basin. The time difference between the neighboring tracks is about 3 days. Although the Nyquist period for the repeat measurements at a given location is 20 days, the measurements made by the neighboring tracks are useful in providing high-frequency (higher than the Nyquist frequency) sampling of the variabilities that have spatial scales larger than the track spacing. For instance, data collected within specified bins (3°x3°) were used to estimate the amplitude and phase of ocean tides at diurnal and semi-diurnal periods (e.g., Schrama and Ray, 1994). In this study we are pushing the limit of T/P data in describing high-frequency, large-scale variabilities.

The T/P Merged Geophysical Data Records were processed with the standard corrections applied, including the tidal and inverted barometer corrections (Callahan, 1994). The

mean sea surface model supplied in the GDR was first removed from individual SSH and the residuals were interpolated to a set of normal points (6.2 km apart) for each repeat track. All the data from October 1992 through December 1997 within a box bounded by 30°S-50°S, 300°E-335°E were used in the analysis. A record time mean was removed from the residual SSH at each normal point. The resultant SSH "anomalies" that reflect only the temporal variations formed the database for the study.

To focus on the large scales we need to filter out the mesoscale variability. A Gaussian-weighted smoothing scheme was applied to the data to create smoothed SSH anomaly maps on a uniform 1°x1° grid every 3 days. At each grid node, all the data within a search window in space and time were used to create a smoothed estimate. The half-weight scale where the Gaussian weight falls to half the maximum value was set to 1° in latitude, 2° in longitude, and 5 days in time. The search window has a dimension of 3° in latitude, 12° in longitude, and 20 days in time. Such a procedure is an efficient scheme for producing gridded maps of large-scale variabilities. As an illustration of the performance of the scheme, the result of using the scheme to sample a relatively fast-moving, large-scale sinusoidal wave is presented in Appendix A. It is shown that large-scale variabilities at frequencies close to the Nyquist of T/P can be sampled qualitatively with a somewhat reduced amplitude.

3. Detection of a 25-day Oscillation

Displayed in Figure 2 is the time series of SSH at 42°S, 316°E, near the center of the study domain. An annual cycle superimposed with energetic high-frequency fluctuations

is prominent. A spatially averaged (over a 4° latitude x 10° longitude box centered on 42°S , 316°E) frequency spectrum is shown in Figure 3. Because the correlation scales of the mapping scheme are comparable to the size of the box, the degree of freedom for the spectrum is low. The formal statistical uncertainty of the spectrum is thus high.

Therefore the spectrum is used only to serve a qualitative purpose for identifying time scales of interests rather than quantitative discussions. An annual peak is clearly shown. A relatively small peak occurs at the semi-annual period, reflecting the known presence of semiannual signals in the region (Fu, 1996; Provost and Le Traon, 1993). Appreciable amount of variance is observed at periods of 20-30 days, 40-50 days, and 80-100 days. The focus of the present study is the phenomenon with periods of 20-30 days that was reported in Weatherly (1993).

A Fourier transform was performed to all the SSH anomaly time series in the study domain and a high-pass filtering was performed by using only the Fourier coefficients with periods shorter than 30 days to reconstruct the time series. Shown in Figure 4 is the high-passed version of Figure 2. Fluctuations with peak-to-trough excursion of 20 cm are seen with seasonal and interannual modulations. The spatial patterns of the high-passed SSH are displayed in Figure 5 for a period of 21 days (March 30-April 20, 1993). The evolving patterns can be characterized by a spatially coherent, counter-clockwise rotating dipole wave. The peak-to-trough sea level amplitude is about 10 cm over a scale of 1000 km. The rms variability computed using the entire 5 years of data has a maximum value of 3 cm located around 42°S , 313°E (Figure 6). The contours of the energy level are somewhat aligned with the contours of f/H , suggesting the barotropic nature of the variability.

The technique of complex-valued empirical orthogonal function (CEOF; e.g., Horel, 1984) was applied to the entire array of high-passed SSH time series in the study domain to investigate the dominant spatial and temporal characteristics of the variability. The amplitude and phase of the leading CEOF are shown in Figure 7. This mode accounts for 38 % of the total variance. The spatial pattern of the amplitude is similar to the rms variability map (Figure 6). The spatial pattern of the phase indicates the rotational character of the variability, with the center of rotation located at 45°S , 318°E , over the Zapiola Rise. The definition of the phase in the CEOF computation indicates that the rotation is counter-clockwise as shown in Figure 5. The temporal evolution of the phase reveals a highly periodic fluctuation with a well-defined frequency of 1 cycle per 25 days. The temporal evolution of the amplitude shows a variety of scales. The low frequency components are visually consistent with the low-frequency modulation of the time series shown in Figure 4. The CEOF analysis indicates that the counter-clockwise rotating dipole wave shown in Figure 5 is a persistent feature of the region with a highly variable amplitude.

The spatial and temporal scales of the dipole wave indicate that the motion field is probably barotropic because the period of baroclinic Rossby waves with a wavelength of 1000 km is on the order of 4 years, much longer than the observed period of 25 days. The 25-day waves observed in the T/P data are probably of the same origin as those observed by the deep current meters reported by Weatherly (1993). The current velocity spectra at 10 m above the ocean bottom at 42.5°S , 315°E show peaks at periods close to 25 days in both the zonal and meridional components (Harkema and Weatherly, 1989).

The coherence between the meridional and zonal components is statistically significant in the 25-day band and the phase indicates a counter-clockwise rotating current. Shown in Figure 8 are the rotary spectra (Gonella, 1972) computed from the data from the velocity records of Harkema and Weatherly (1989). The dominance of the counter-clockwise component at periods close to 25 days is clearly shown at both 10 m and 198 m above the ocean bottom. The counter-clockwise component of velocities at the two depths are highly coherent at periods from 20-50 days (0.95, above the 95% confidence level with 5 degrees of freedom) with small phase difference (Figure 9). The spectral analysis suggests that a vertically coherent, counter-clockwise rotating current with a period of about 25 days does exist near the ocean bottom, consistent with the assertion that the T/P observed 25-day waves are barotropic and involve uniform motion of the entire water column.

The speed of the current associated with the wave is on the order of 1 cm/s, computed from the sea surface slope of a 10 cm change over a distance of 1000 km based on geostrophy. However, because of the movement of the entire water column at this speed, the variability of the mass transport caused by the wave is about 50 Sv, a significant fraction of the transport of the mean flow in the region (Saunders and King, 1995).

4. Theoretical Considerations

The f/H contours (Figure 6) are indicators of the gradient of barotropic potential vorticity in the region. Some of the contours are closed (or semi closed) around the Zapiola Rise. The fact that the dipole waves are essentially rotating around the Zapiola Rise suggests

their origin as topographically-controlled Rossby waves dictated by the f/H contours. A linearized barotropic potential vorticity equation can be written as

$$\frac{\partial}{\partial t} \left(\nabla^2 \eta - \frac{f^2}{gH} \eta \right) + H J \left(\eta, \frac{f}{H} \right) = 0 \quad (1)$$

where η is the sea surface height anomaly, H is the ocean depth (a variable), f is the Coriolis parameter, and J is the Jacobi operator. For the scales of the observed waves, which are on the order of 1000 km, the vortex stretching term f^2/gH can be neglected when compared to $\nabla^2 \eta$. The geometry of the solution is dictated by the second term of (1), the advection of the potential vorticity. Given the semi-closed contours of f/H and the apparent rotation of the waves around the Zapiola Rise, we approximate f/H by an axial symmetric function and convert Eq. (1) into polar coordinates centered on the Zapiola Rise:

$$\frac{\partial}{\partial t} \left(\frac{\partial^2 \eta}{\partial r^2} + \frac{1}{r} \frac{\partial \eta}{\partial r} + \frac{1}{r^2} \frac{\partial^2 \eta}{\partial \theta^2} \right) - \frac{H}{r} \frac{\partial \eta}{\partial \theta} \frac{\partial}{\partial r} \left(\frac{f}{H} \right) = 0 \quad (2)$$

We seek azimuthally propagating wave solution,

$$\eta = p(r) \exp[i(s\theta - \omega t)],$$

where s is the azimuthal wave number and ω is the wave frequency. We define

$$\beta_e \equiv H \frac{\partial}{\partial r} \left(\frac{f}{H} \right),$$

which represents an equivalent beta effect, and assume that β_e is a constant. Eq. (2) then becomes

$$\frac{\partial^2 p}{\partial r^2} + \frac{1}{r} \frac{\partial p}{\partial r} - \frac{s^2}{r^2} p + \frac{s \beta_e}{r \omega} p = 0 \quad (3)$$

With $z \equiv 2\sqrt{r}$, (3) can be transformed to

$$\frac{\partial^2 p}{\partial z^2} + \frac{1}{z} \frac{\partial p}{\partial z} - \frac{4s^2}{z^2} p + \frac{s \beta_e}{\omega} p = 0, \quad (4)$$

which is a Bessel's equation. A general solution to (4) can be written as

$$\eta = \sum_{s=0}^{\infty} A_s \exp[i(s\theta - \omega t)] J_{2s}(2k\sqrt{r}), \quad (5)$$

where $k^2 = s\beta_e / \omega$. Note that β_e is positive in this case, namely, f/H is increasing with r . This leads to a counter-clockwise rotating wave solution as observed (s and ω are of the same sign). If β_e is negative, the wave solution would show clock-wise rotation.

Because the observed waves assume a dipole structure, we set $s = 1$. The fact that the observed waves are confined to the Argentine Basin where there are closed f/H contours

leads us to require the solution to be confined to a circular region with a radius of L . This requirement gives rise to the following dispersion relation:

$$J_2(2k\sqrt{L}) = 0, \text{ or } 2k\sqrt{L} = 5.15 \quad (6)$$

From (6) the wave period is given by

$$T = \frac{2\pi}{\omega} = \frac{5.15^2 \pi}{2L\beta_e} \quad (7)$$

The value of β_e estimated from Figure 6 (the unit of the contour interval is $1.46 \times 10^9 \text{ sec}^{-1} \text{ m}^{-1}$) is about $3.3 \times 10^{11} \text{ sec}^{-1} \text{ m}^{-1}$ in the vicinity of the Zapiola Rise. Physically, L is determined by the scale over which the f/H contours either change abruptly (i.e., a potential vorticity barrier) or flatten out (i.e., no potential vorticity gradient to support Rossby waves). Estimated from Figure 6, L is on the order of 500 km. With these values for L and β_e , $T \approx 29$ days ($L=580$ km would make $T=25$ days). Figure 10 shows that T is not particularly sensitive to either L or β_e within a reasonable range of values. The observed wave period of 25 days can be readily explained by the theory. Shown in Figure 11 is the wave function with the above parameters for $s=1$. The spatial patterns of the observed waves can also be qualitatively accounted for by the theory.

The theoretical analysis discussed above suggests that the observed waves are signatures of a normal mode associated with the local topography. To verify the existence of such a mode in a more realistic setting, a numerical model was run to simulate the variabilities of the Argentine Basin. This is a barotropic model with a spatial resolution of $0.5^\circ \times 0.5^\circ$,

covering the domain of 75° W- 15° W and 20° S- 60° S. All the model boundaries are closed. The eddy viscosity coefficient used in the model is $500 \text{ m}^2/\text{s}$ and this value is increased to $5000 \text{ m}^2/\text{s}$ near the model's open boundaries in order to minimize spurious boundary Kelvin waves. The model topography is based on the ETOPO5 database. The NCEP daily wind was used to drive the model from January 1, 1990 to December 31, 1997. The 8-year mean wind was removed because the mean circulation is not of interests to the study. CEOF analysis was applied to the resulting barotropic stream function. The first three leading modes account for 62% of the variance. All three are barotropic Rossby wave modes. The first two, with periods of 10-22 days, are not confined to the region of the Zapiola Rise. The third mode, accounting for 10% of the variance, has a distinct period of 22 days with spatial patterns similar to the observed 25-day waves (Figure 12). The degree of resemblance in both the spatial phase and amplitude distribution between Figure 7 and Figure 12 is fairly convincing. The peak-to-trough sea level amplitude associated with the mode is about 8 cm, comparable to the observation. However, it is not clear why the first two modes of the model simulation are not observed in the data. The high-order CEOF's of the high-passed sea level observations do not show anything resembling them.

5. Discussion and Conclusion

Satellite altimetry provides the first synoptic view of the large-scale intraseasonal variability of the ocean. Due to the sparseness of in-situ observations, our knowledge of the spatial extent and pattern of the variability has been sketchy. T/P altimeter is the first that has sufficient accuracy and sampling capability for observing the variability. This

paper presents a case study of the Argentine Basin where the intraseasonal variability is particularly energetic. Near the highest frequencies resolvable by T/P, a 25-day rotating dipole wave is detected. The half wavelength of the wave is about 1000 km with a peak-to-trough amplitude of 10 cm. Due to the closeness of the period to the Nyquist period of T/P (20 days), the amplitude may have been underestimated. The wave rotates counter-clockwise around the Zapiola Rise. The spatial distribution of wave amplitude is correlated with the local f/H contours. The spatial and temporal characteristics of the wave can be explained by a solution to the linearized barotropic vorticity equation. The observed wave appears to be a normal mode associated with the local f/H geometry. Deep current meter observations provide corroborative evidence for the altimetric observations and the interpretation of them as barotropic waves.

Observational as well as theoretical and numerical studies of the Argentine Basin have indicated the existence of an anticyclonic (counter-clockwise) mean circulation around the Zapiola Rise (Flood and Shor, 1988; Saunders and King, 1995; Weatherly, 1993; Dewar, 1998; de Miranda et al., 1999). The transport of this anticyclone is estimated to be 140 Sv. Theoretical and modeling analysis suggests that this mean flow is driven by eddies trapped inside closed f/H contours around the Zapiola Rise. The counter-clockwise dipole wave observed in the present study might have some interactive relationship with the anticyclonic mean flow.

In an effort of investigating the relationship between the variability of the wind field and the observed sea level variability, we have examined the time series of wind stress and its curl in the Argentine Basin. Data from both the NCEP analysis and the ERS

scatterometer were used for the analysis. There was no evidence for any significant wind variability at periods close to 25 days. Wavelet analysis was also performed to the variance of wind stress curl at periods close to 25 days. We found no significant correlation between the variability of the wave amplitude with the variability of the wind stress curl. Therefore we are not able to establish any relationship between wind forcing and the observed wave. Since the wave appears to be a normal mode of the basin, it is probably excited as a resonant response to random forcing. The variation of the wave's amplitude is not directly controlled by the amplitude of the forcing.

Recent modeling studies (Fukumori et al., 1998; Stammer et al., 1999; Tierney et al., 1999) have suggested that there is significant amount of variability of sea level and ocean circulation at periods shorter than the Nyquist of T/P . These high-frequency variabilities could be aliased into lower frequencies and cause some errors in the present analysis. However, such variability has an rms amplitude of 1-2 cm in the Argentine Basin and should not have a significant effect on the result of the paper.

Acknowledgements

The current meter data were kindly provided by Dr. Georges Weatherly of the Florida State University. The research presented in the paper was partly carried out by the Jet Propulsion Laboratory, California Institute of Technology, under contract with the National Aeronautic and Space Administration. Support from the TOPEX/POSEIDON Project is acknowledged. The effort of Bo Qiu was supported by TOPEX/POSEIDON Extended Mission through Contract 960889 issued to the University of Hawaii.

Appendix A.

To investigate how well T/P is able to sample a fast moving, large-scale anomaly, we conducted an experiment in which a simulated plane wave was sampled at real T/P measurement times and locations. The simulated observations were then used to reconstruct the wave for comparison to the truth. The simulated sea surface height anomaly is given by

$$h = A \sin\left(\frac{2\pi}{L_x}x + \frac{2\pi}{L_y}y - \frac{2\pi}{P}t\right),$$

where $A=5$ cm, $L_x=25^\circ$, $L_y=15^\circ$, $P=25$ days. This wave was sampled over 40 days in the Argentine Basin at real T/P measurement times and locations. The simulated data were processed using the Gaussian smoothing scheme described in Section 2 to produce $1^\circ \times 1^\circ \times 3$ day maps. Shown in Figure A.1 is a comparison of the simulated T/P sampled wave with the truth for 4 consecutive 3 day maps. The correlation between each pair is greater than 0.85. The rms difference is about 2 cm. The wave amplitude is under sampled by the simulated T/P observations, but the basic pattern and its propagation characteristics are faithfully reproduced. This has demonstrated the capability of T/P in retrieving large-scale temporal variabilities at time intervals shorter than the 10-day repeat period. This experiment indicates that the observed dipole waves might have an amplitude larger than revealed by the T/P observations.

Figure Captions

Figure 1. Root-mean-squares variability of sea surface height measured by T/P (top) and simulated by an ocean general circulation model (bottom). Both were filtered to retain energy at spatial scales larger than 1000 km and temporal scales from 20- 100 days. (from Fu and Smith, 1996).

Figure 2. Time series of sea surface height anomaly at 42°S, 316°E.

Figure 3. Average of the frequency spectra computed at the 1°x1° grids. The average is performed over a 4° latitude x 10° longitude box centered on 42°S, 316°E.

Figure 4. High-pass filtered version of Figure 2. Variability with periods longer than 30 days is removed.

Figure 5. Snap shots of high-passed sea surface height anomaly 3 days apart from March 30 to April 20, 1993.

Figure 6. RMS amplitude of the high-passed sea surface height variability (thick contours in unit of mm). The f/H contours in unit of $1.46 \times 10^{-9} \text{ sec}^{-1} \text{ m}^{-1}$ are shown by the thin lines.

Figure 7. The first complex-valued empirical orthogonal function for the high-passed sea surface height anomalies. Top left: the spatial distribution of the amplitude. Bottom left:

the temporal evolution of the amplitude. The multiplication of two left panels gives the amplitude of the sea surface height in mm. Top right: the spatial distribution of the phase in degrees. Bottom right: temporal evolution of the phase in degrees.

Figure 8. The rotary components of the frequency spectra of the velocity records from moored current meters at 10 m (right) and 198 m (left) from the bottom of the ocean. The clockwise component is shown by the solid lines and counter-clockwise component by the dotted lines.

Figure 9. The amplitude (left) and phase (right) of the coherence between the counter-clockwise component of the current velocity records at 10 m and 198 m depths.

Figure 10. The wave period as a function of L for three values of β_e .

Figure 11. The spatial pattern of the solution represented by Eq. (5) with $s=1$.

Figure 12. The spatial patterns of the amplitude (upper panel) and the phase (lower panel) for the 3rd CEOF of the model simulation.

Figure A.1 Simulated sinusoidal wave (upper panels) versus its reconstruction based on values sampled by T/P along its ground tracks (lower panels). The box represents the domain of the study with the vertical axis in latitude and horizontal axis in longitude.

References

- Brink, K.H., Evidence for Wind-Driven Current Fluctuations in the Western North Atlantic. *J. Geophys. Res.*, 94 (C2), 2029-2044, 1989.
- Callahan, P. S., 1994: *TOPEX/POSEIDON GDR User's Handbook*, JPL D-8944, Jet Propulsion Laboratory, Pasadena, CA.
- Chao, Y., and L.-L. Fu, 1995: A comparison between the TOPEX/POSEIDON data and a global ocean general circulation model during 1992-93. *Journal of Geophysical Research*, 100, 24965-24976.
- De Miranda, A.P., B. Barnier, and W.K. Dewar, 1999: Eddy-driven flow over topography: the case of the Zapiola Anticyclone in the Argentine Basin.
- Dewar, W.K., 1998: Topography and barotropic transport control by bottom friction, *J. Mar. Res.*, 56, 295-328.
- Enfield, D.B., The intraseasonal oscillation in eastern Pacific sea levels: how is it forced? *J. Phys. Oceanogr.*, 17, 1860-1867, 1987.
- Flood, R.D., and A.N. Shor, 1988: Mud waves in the Argentine Basin and their relationship to regional bottom circulation patterns, *Deep-Sea Res.*, 35, 943-971.
- Fu, L.-L. 1996: The circulation and its variability of the South Atlantic Ocean: first results from the TOPEX/POSEIDON Mission, in *The South Atlantic: Present and Past Circulation*, pp. 63-82, G. Wefer et al., (eds.), Springer-Verlag, 644pp.
- Fu, L.-L., and R.A. Davidson, 1995: A note on the barotropic response of sea level to time-dependent wind forcing, *Journal of Geophysical Research*, 100, 24955-24963.

Fu, L.-L., E. J. Christensen, C.A. Yamarone, M. Lefebvre, Y. Menard, M. Dorrer, and P. Escudier, 1994: TOPEX/POSEIDON Mission Overview, *Journal of Geophysical Research*, *99*, 24369-24381.

Fu, L.-L., and J. Vazquez, 1988: On correcting radial orbit errors for altimetric satellites using crossover analysis. *Journal of Atmospheric and Oceanic Technology*, *5*, 466-471.

Fu, L.-L., and R.D. Smith, 1996: Global ocean circulation from satellite altimetry and high- resolution computer simulation. *Bull. Amer. Meteorolog. Soc.*, *77*, 2625-2636.

Fukumori, I., R. Raghunath, and L.-L. Fu, 1997: The nature of global large-scale sea level variability in relation to atmospheric forcing: A modeling study, *J. Geophys. Res.*, *103*, 5493-5512.

Garzoli, SL, Garraffo, Z (1989) Transports, frontal motions and eddies at the Brazil-Malvinas confluence as revealed by inverted echo sounders. *Deep-Sea Res.* *36*: 681-703.

Garzoli, SL, Giulivi, C (1994) What forces the variability of the south western Atlantic boundary currents? *Deep-Sea Res.* *41*: 1527-1550.

Gonella, J., 1972: A rotary-component method for analyzing meteorological and oceanographic vector time series, *Deep-Sea Res.*, *18*, 775-788.

Harkema, R., and G.L. Weatherly, 1989: *A compilation of moored current meter data in the Argentine Basin April 25, 1987- March 14, 1988*, Tech. Rept. CMF-89-01, Dept. of Oceanography, Florida State University, Tallahassee, FL, 64 pp.

Horel, J.P., 1984: Complex principal component analysis: theory and examples, *J. Clim. Appl. Meteorol.*, *23*, 1600-1673.

Koblinsky, C. J., P. P. Niiler, and W. J. Schmitz, Jr., 1989: Observations of Wind-Forced Deep Ocean Currents in the North Pacific, *J. Geophys. Res.*, *94*, 10,773-10,790.

Luther, D.S., A.D. Chave, J.H. Filloux, and P.F. Spain, Evidence for Local and Nonlocal Barotropic Responses to Atmospheric Forcing During Bempex. *Geophys. Res. Lett.*, *17*(7), 949-952, 1990.

Matano, RP, Schlax, MG, Chelton, DB (1993) Seasonal Variability in the Southwestern Atlantic. *J. Geophys. Res.*. *98*: 18027-18035.

McPhaden, M.J., Monthly period oscillations in the Pacific North Equatorial Countercurrent, *J. Geophys. Res.*, *101*, 6337-6359, 1996.

Niiler, P.P., J. Filloux, W.T. Liu, R.M. Samelson, J.D. Paduan, and C.A. Paulson, Wind-Forced Variability of the Deep Eastern North Pacific: Observations of Seafloor Pressure and Abyssal Currents. *J. Geophys. Res.*, *98* (C12), 22,589-22,602, 1993.

Olson, DB, Podesta, GP, Evans, RH, Brown, OB (1988) Temporal variations in the separation of Brazil and Malvinas Currents. *Deep-Sea Res.* *35*: 1971-1990.

Provost, C. and P.-Y. Le Traon, Spatial and Temporal Scales in Altimetric Variability in the Brazil-Malvinas Current Confluence Region: Dominance of the Semiannual Period and Large Spatial Scales. *J. Geophys. Res.*, *98*(C10), 18037-18051, 1993.

Samelson, R.M., Evidence for Wind-Driven Current Fluctuations in the Eastern North Atlantic. *J. Geophys. Res.*, *95* (C7), 11,359-11,368, 1990.

Saunders, P.M., and B.A. King, 1995: Bottom currents derived from a shipborne ADCP on the WOCE Cruise A11 in the South Atlantic, *J. Phys. Oceanogr.*, *25*, 329-347.

Schrama, E.J.O., and R.D. Ray, A preliminary tidal analysis of TOPEX/POSEIDON altimetry, *J. Geophys. Res.*, *99*, , 1994.

Stammer, D., C. Wunsch, and R.M. Ponte, 1999: De-Aliasing of Global High Frequency Barotropic Motions in Altimeter Observations, submitted to *Geophys. Res. Letts.*

Tapley, B. D., et. al., 1994 a: Precision orbit determination for TOPEX/POSEIDON, *J. Geophys. Res.*, 99(C12), 24,383-24,404.

Tierney, C., J. Wahr, F. Bryan, and V. Zlotnicki, 1999: Short-period oceanic circulation: implications for satellite altimetry, to be submitted.

Wagner, C.A. and C.K. Tai, Degradation of ocean signals in satellite altimetry due to orbit removal processes. *J. Geophys. Res.*, 99, 16255-16267, 1994.

Weatherly, G.L., 1993: On deep-current and hydrographic observations from a mudwave region and elsewhere in the Argentine Basin, *Deep-Sea Res.*, 40 (PartII), 851-858.

Witter, D. L., and Gordon, A. L. (1999). Interannual variability of the South Atlantic Circulation from four years of TOPEX/POSEIDON altimeter observations. *J. Geophys. Res.* (submitted).

Wunsch, C., and A. E. Gill, 1976: Observations of equatorially trapped waves in Pacific sea level variations, *Deep-Sea Res.*, 23, 371-390.

LARGE SCALE 20-100 DAY SEA SURFACE HEIGHT VARIABILITY

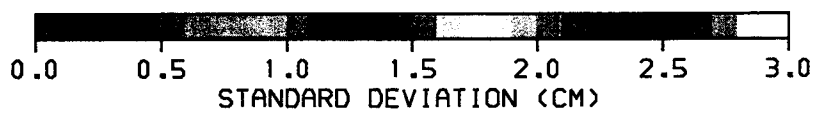
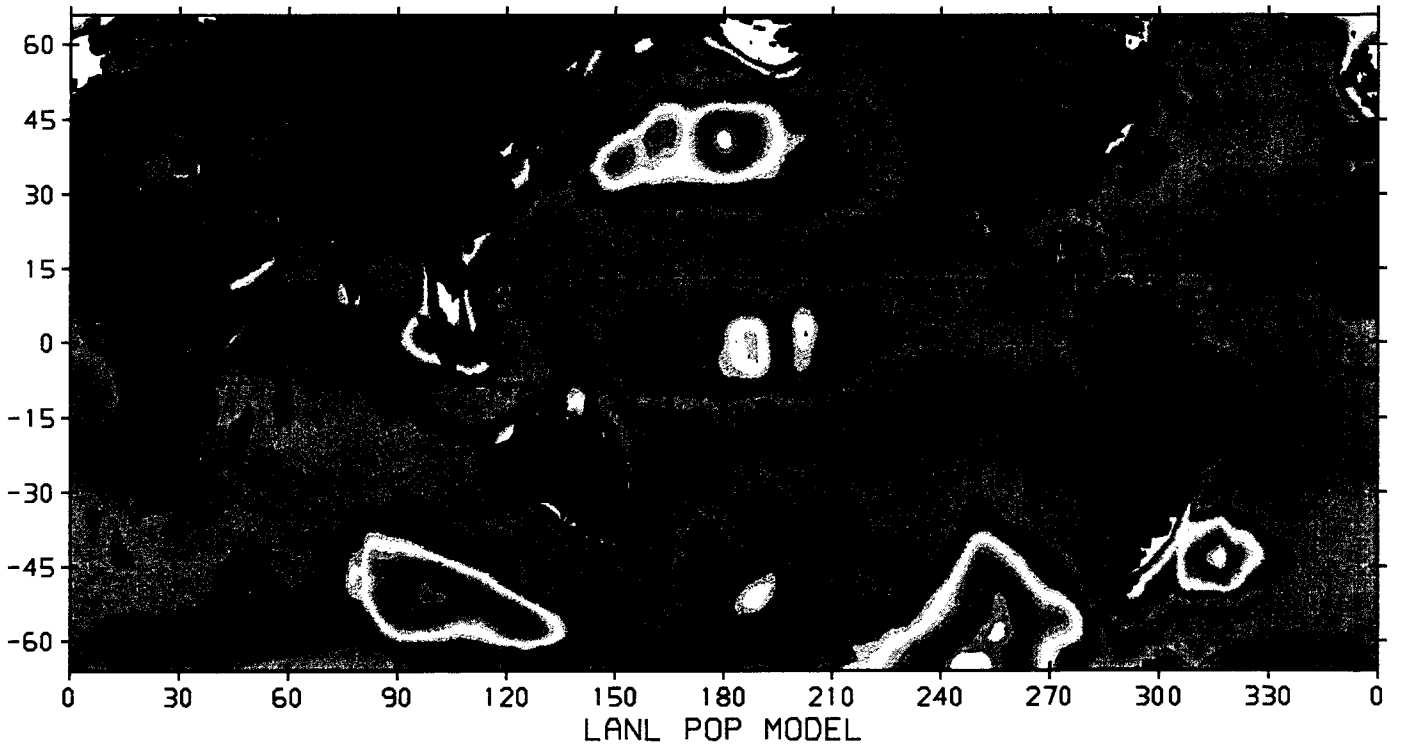
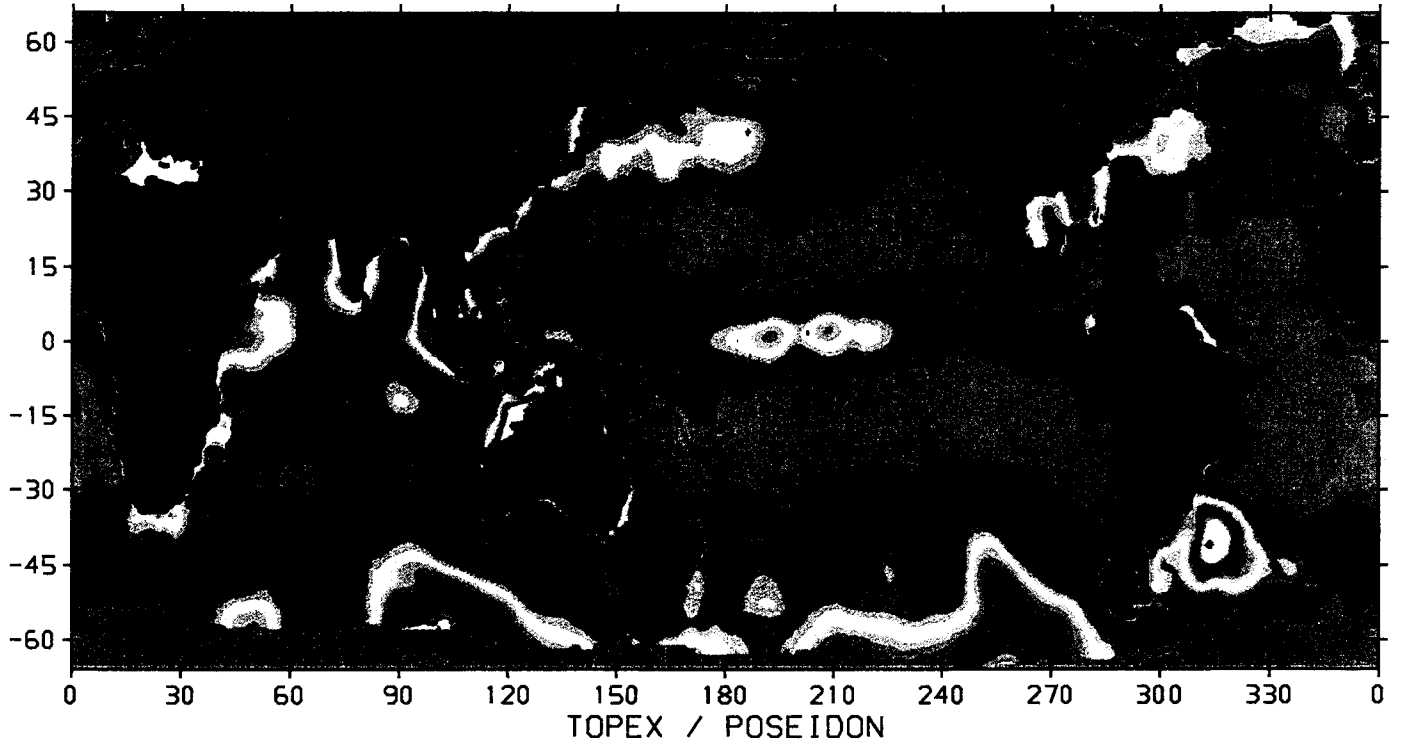


Fig. 1

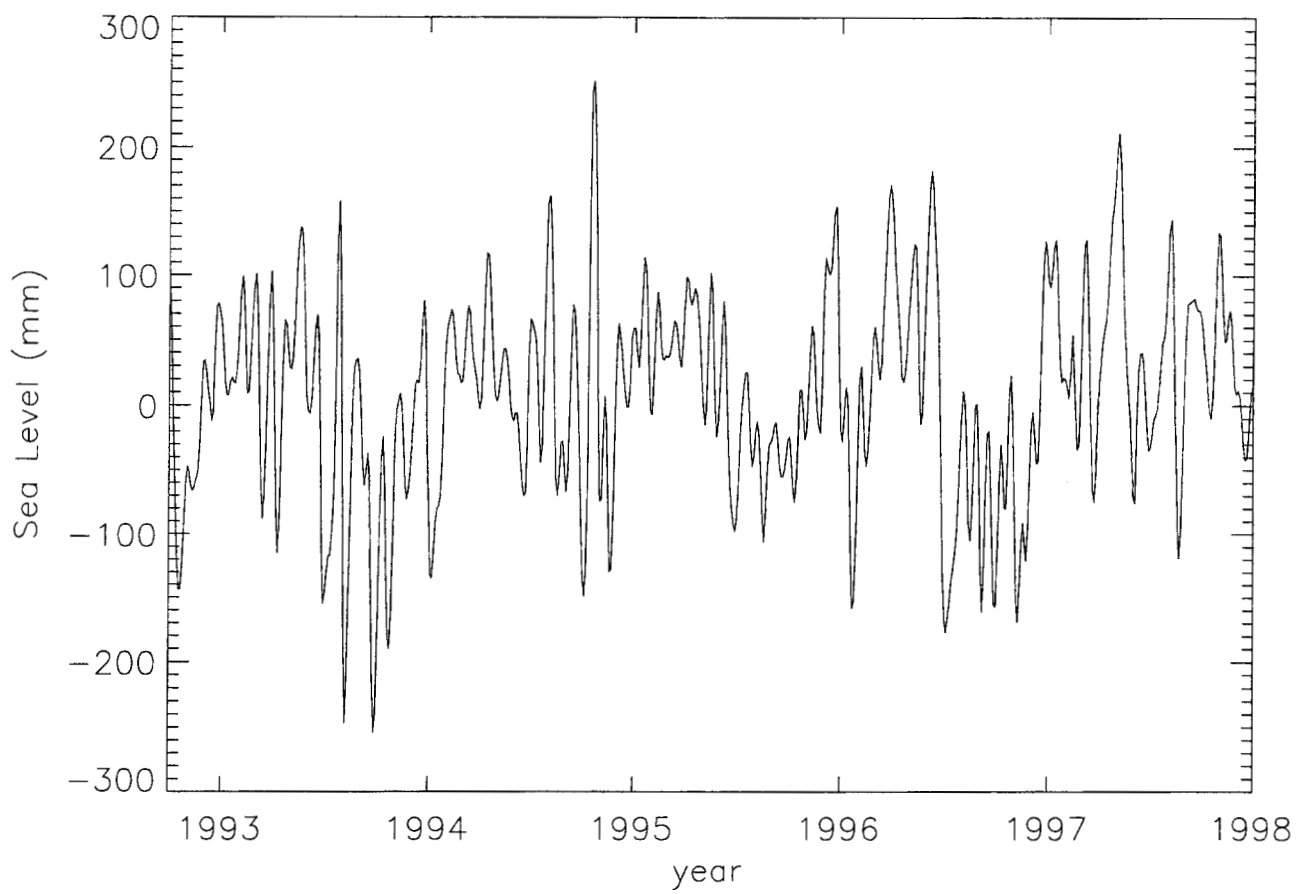


Fig. 2

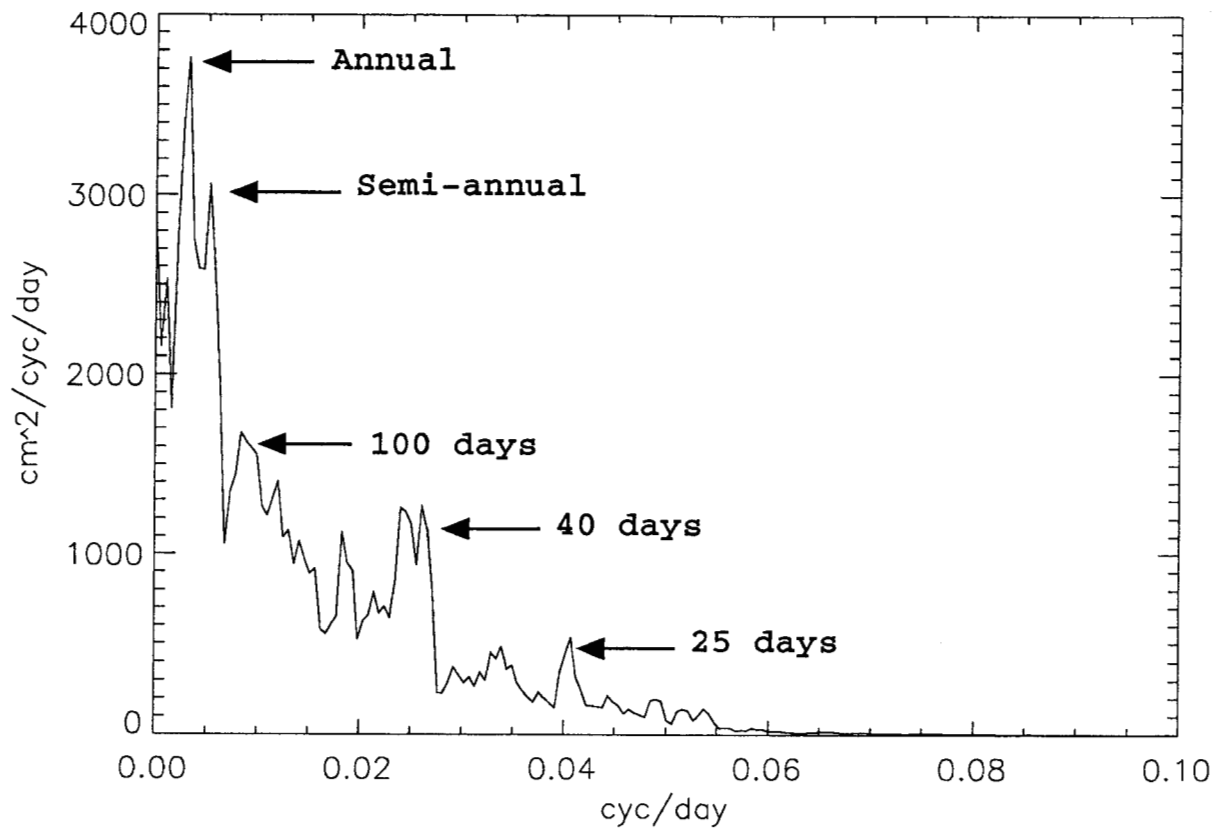


Fig. 3

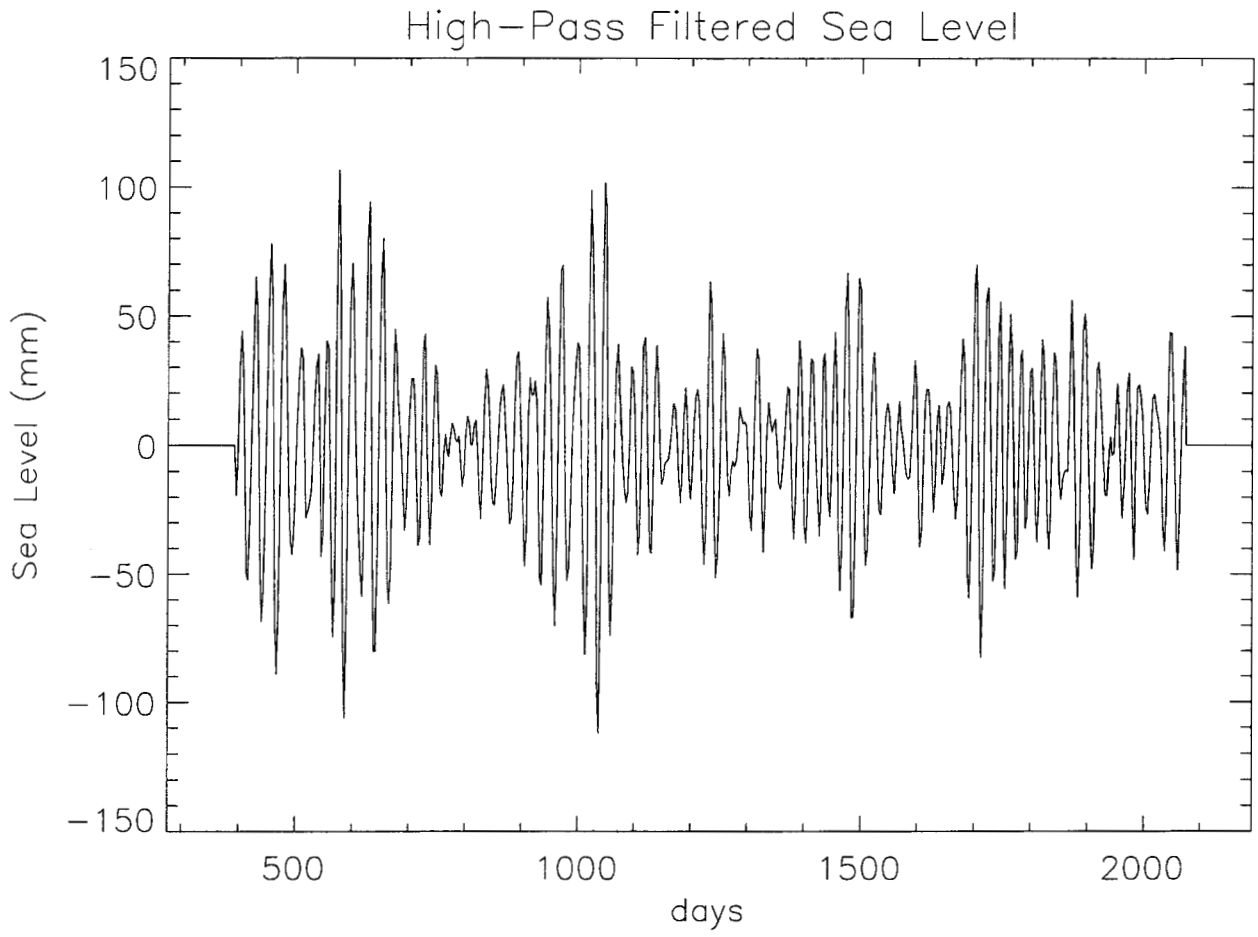


Fig. 4

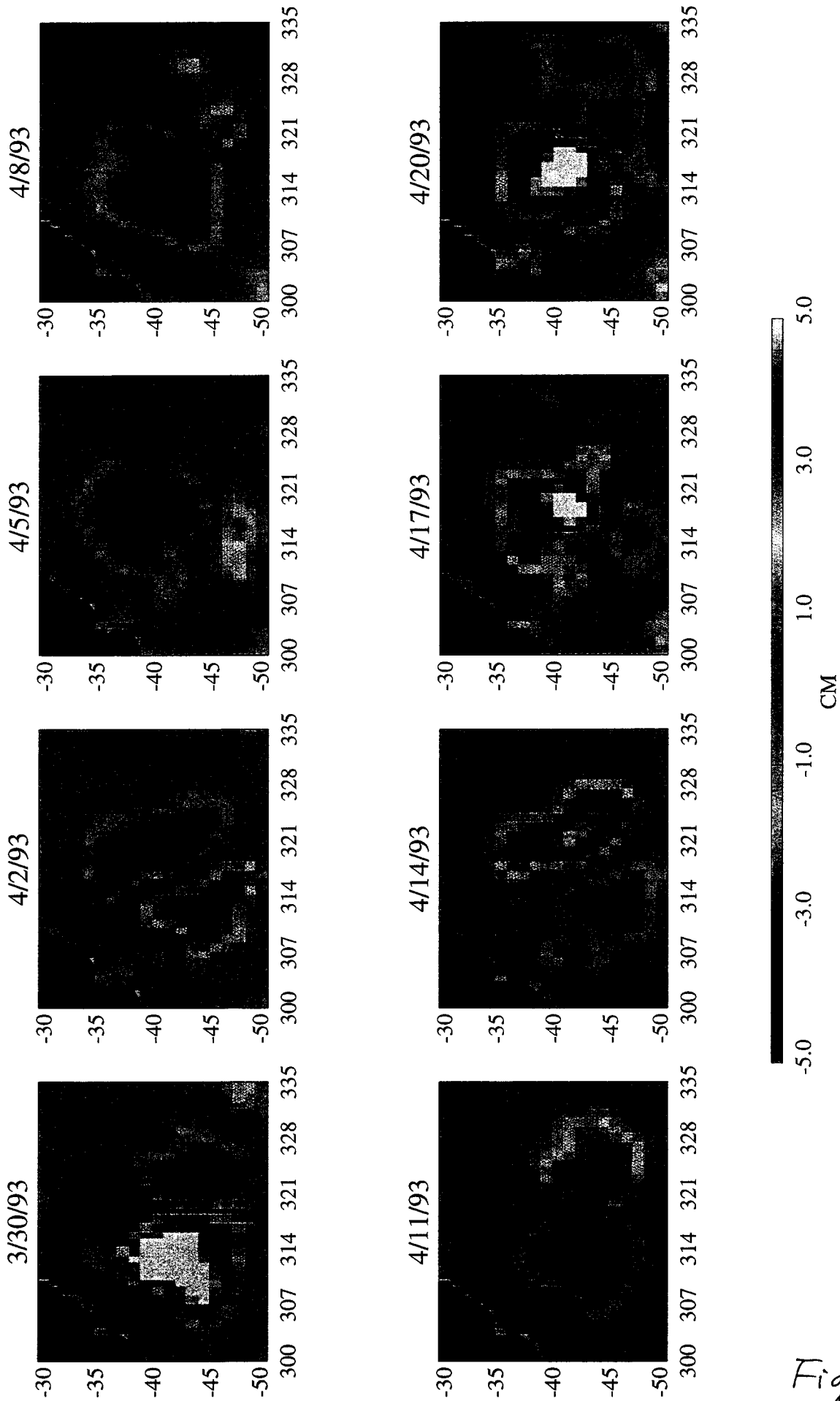


Fig. 5

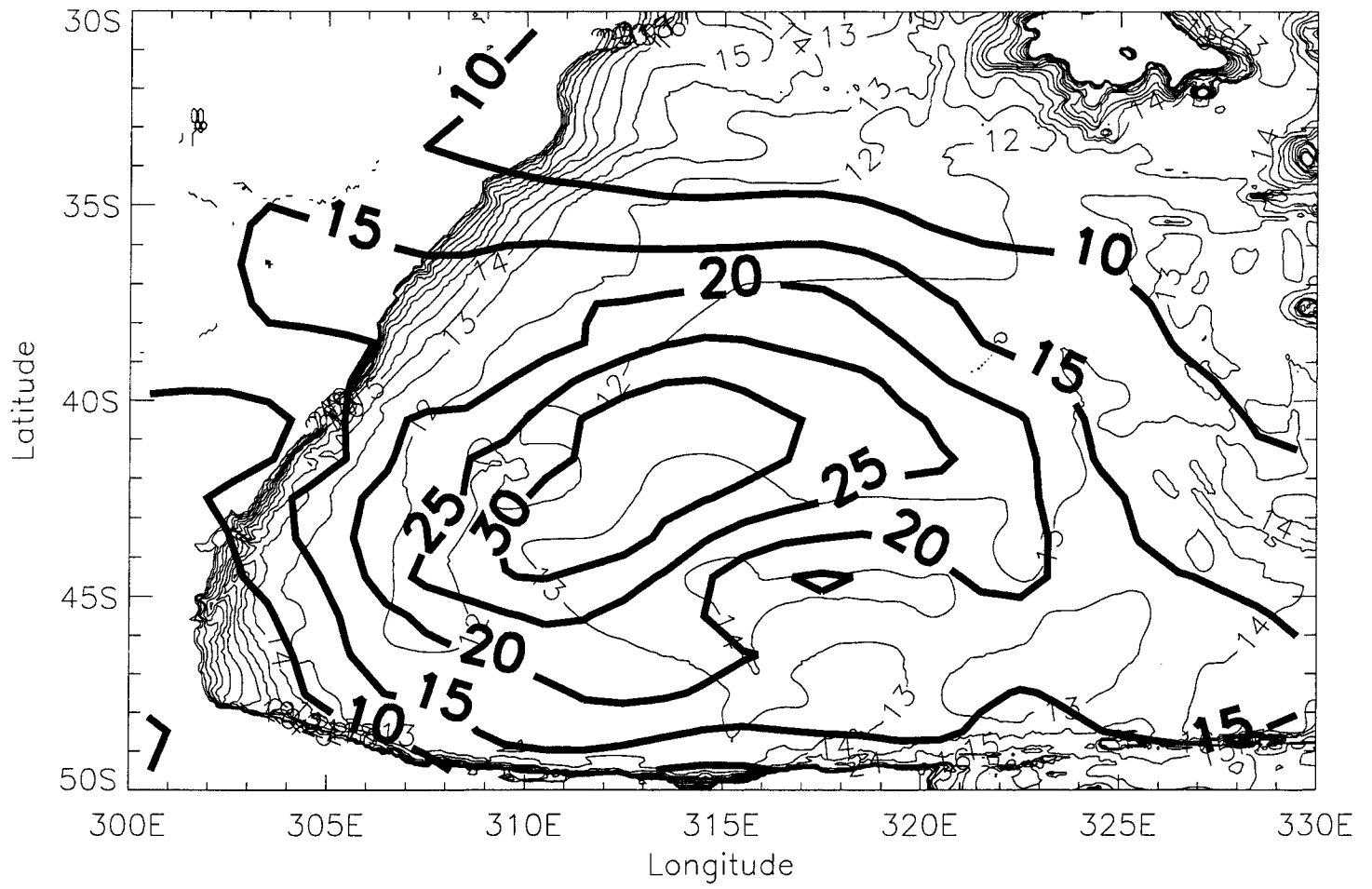


Fig. 6

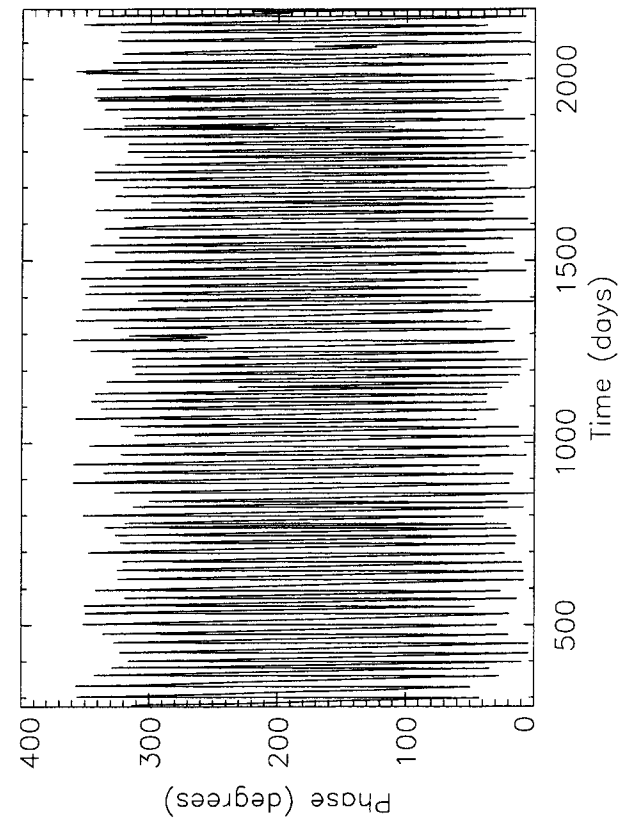
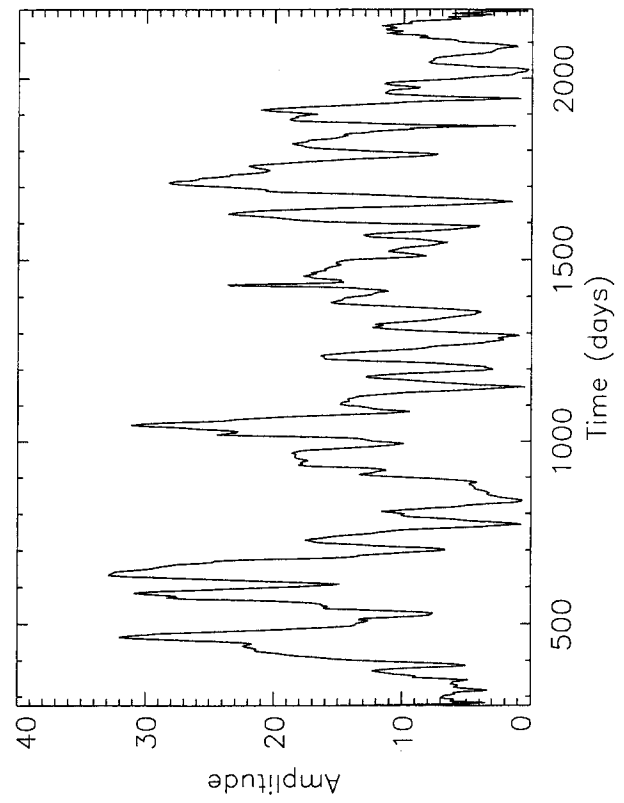
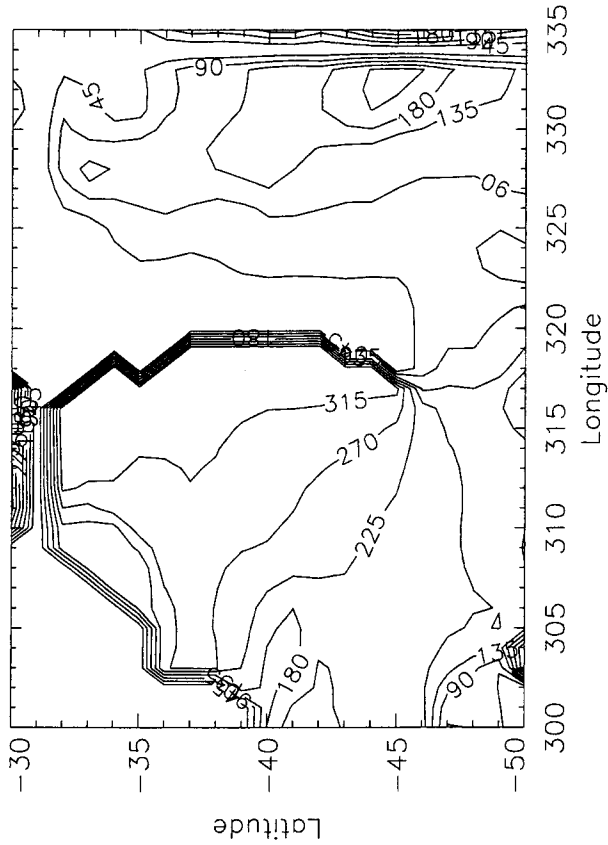
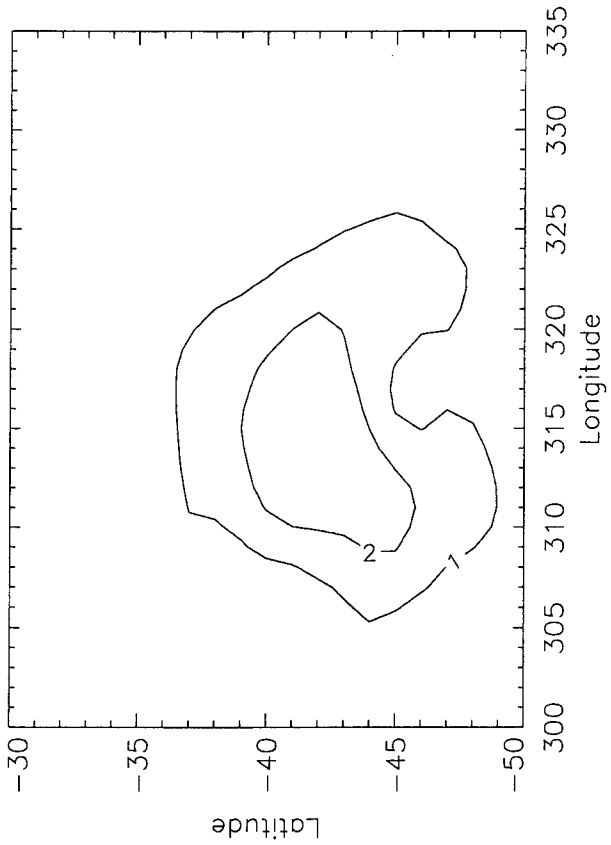


Fig. 7

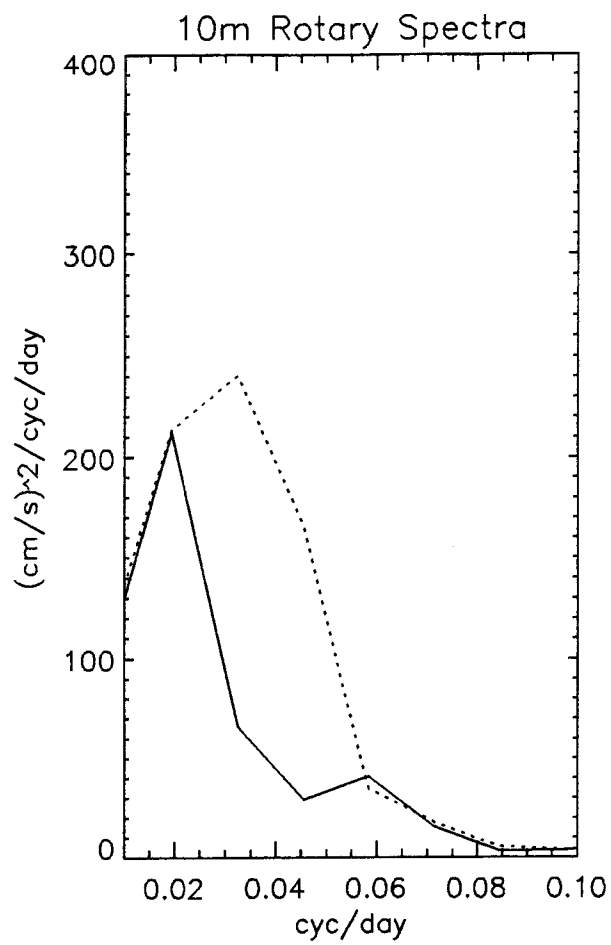
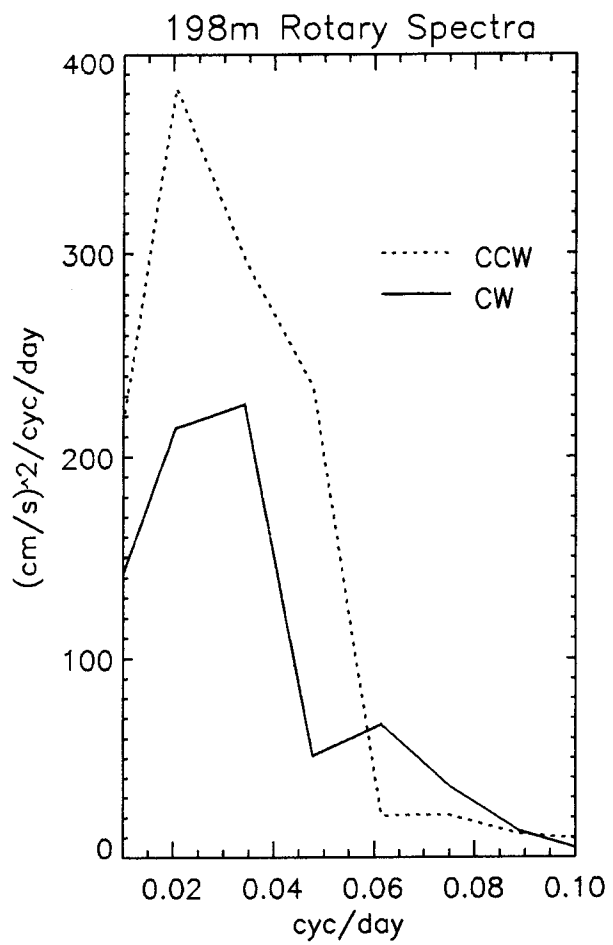


Fig. 8

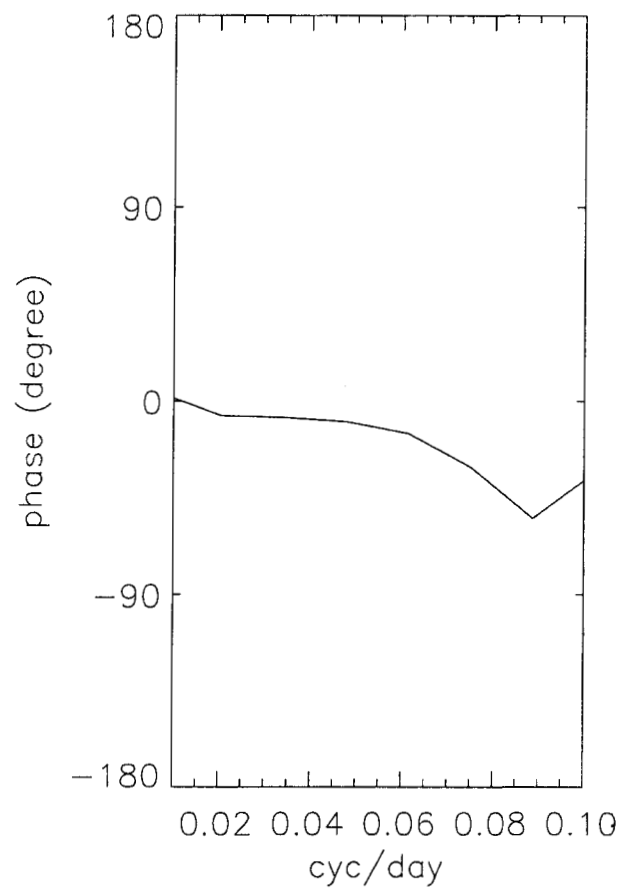
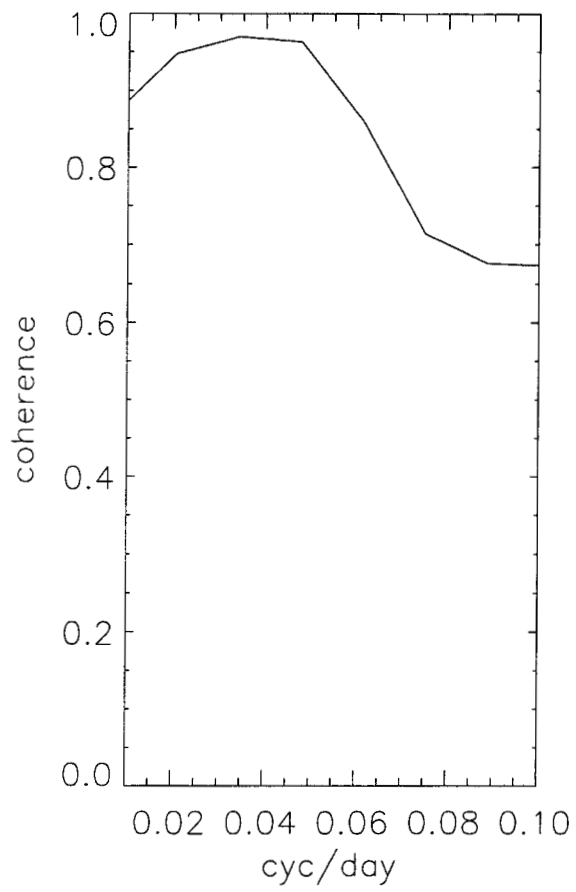


Fig. 9

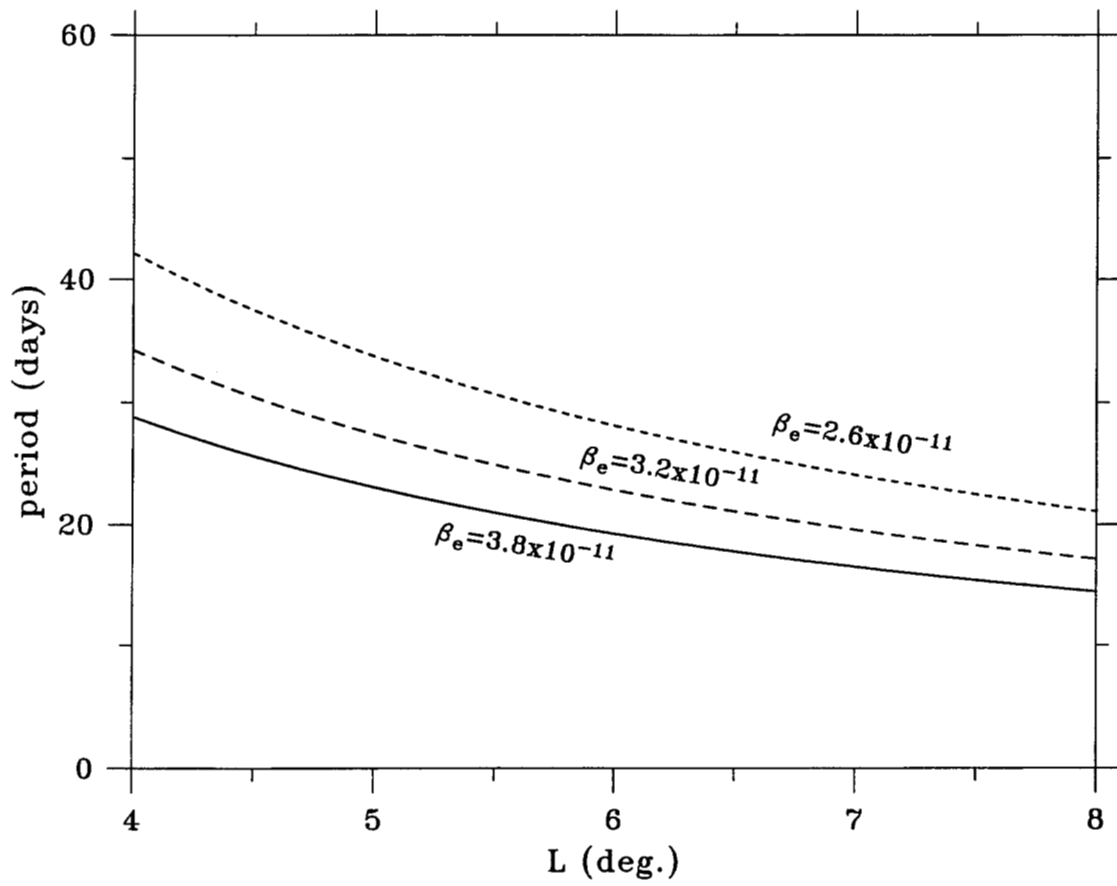


Fig. 10

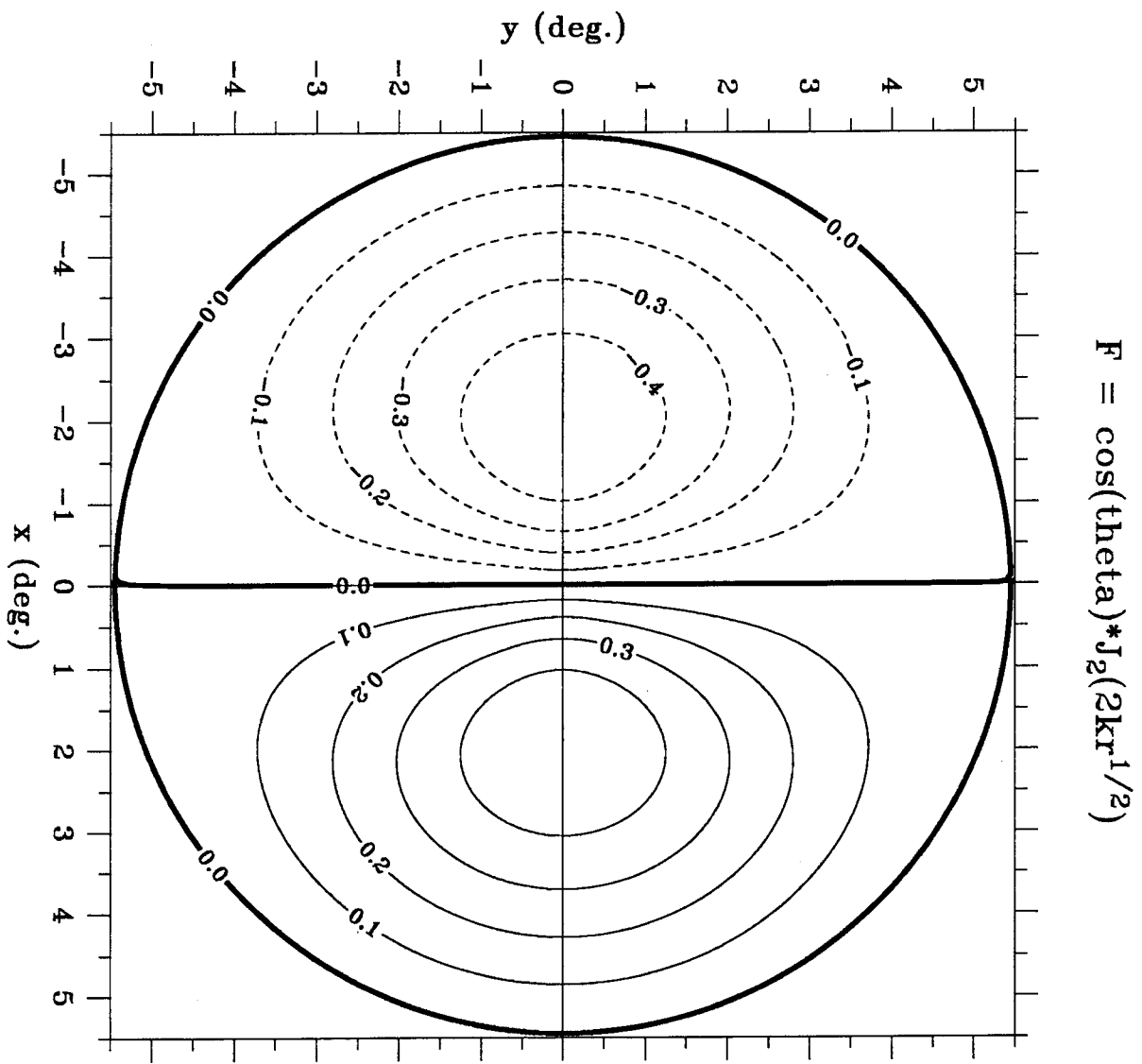


Fig. 11

Spatial amplitude and phase of 3rd CEOF mode

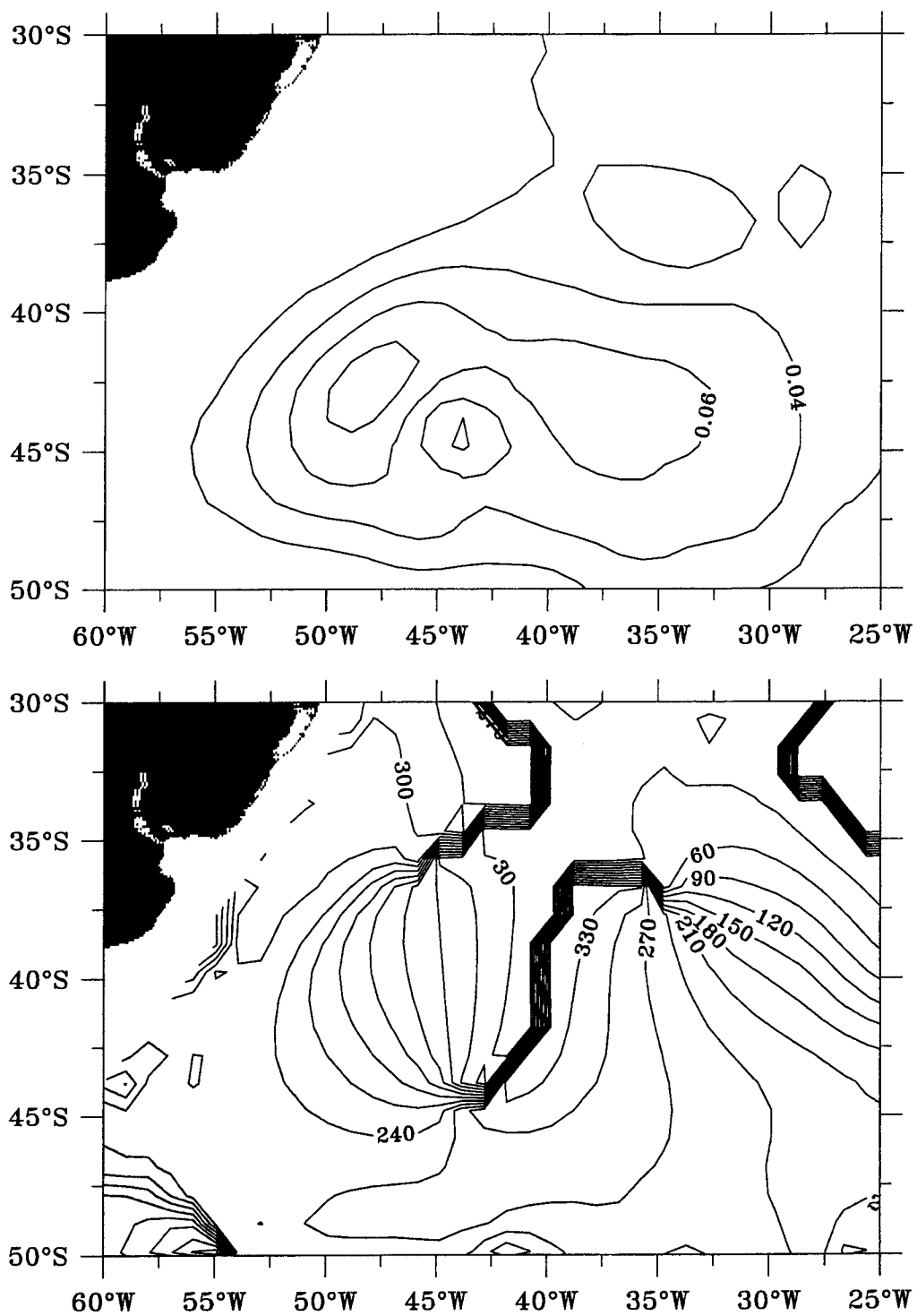


Fig. 12

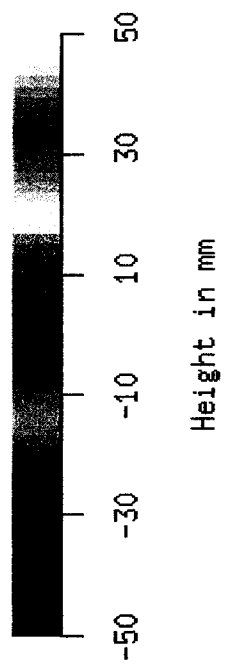
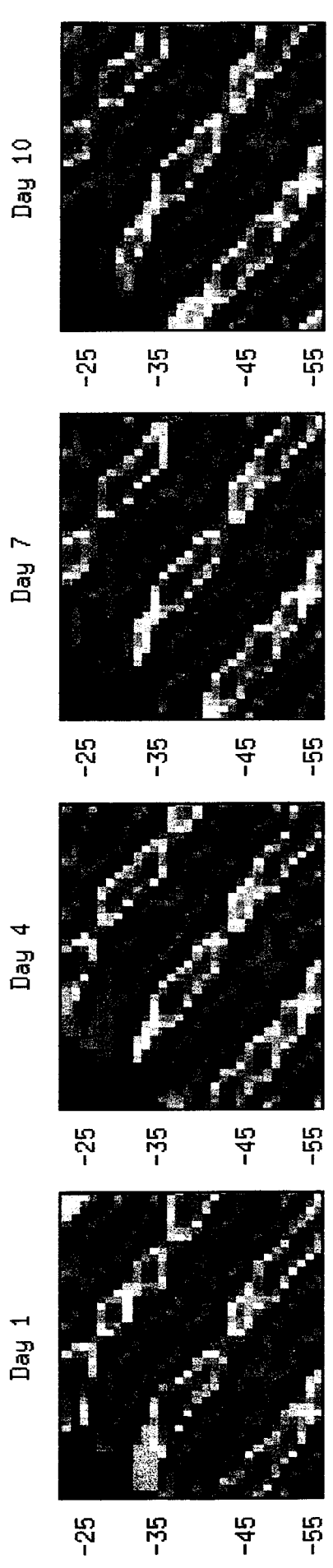
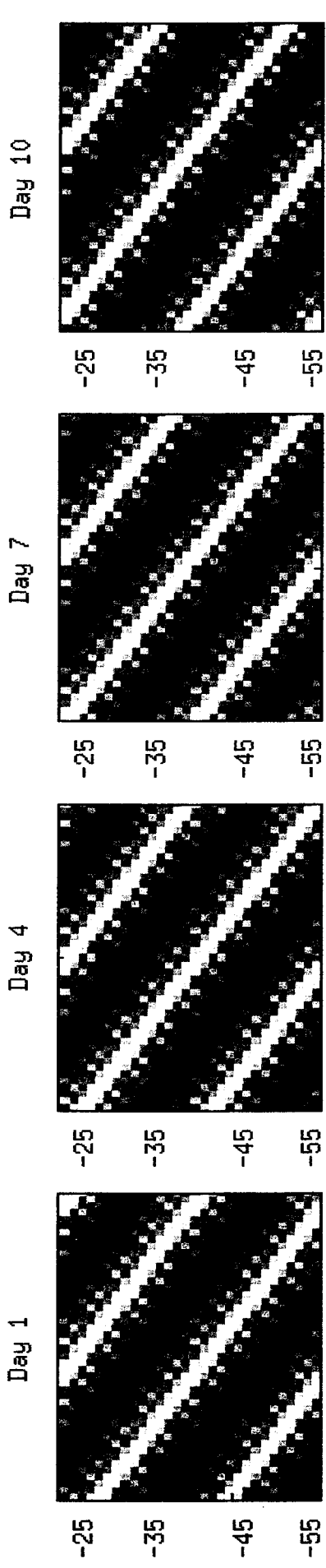


Fig. A.1